Chapter 5

THE GENERATION OF SEA-SALT AEROSOLS

Terns speckled brown
Gulls pearly gray
Flying through the rainbow
Amidst the ocean spray.

Patricia M. Klempa, *OCEAN BEAUTY*

The results reported in the previous chapters can now be used to fulfill the next goal of this study to modify the existing generation function of sea-salt aerosols and compute sea-salt aerosol loadings. Using the resulting global fields of sea-salt aerosols, it would be possible to estimate the contribution of sea-salt aerosols to various climate processes. This chapter describes the approaches used to modify the generation function, documents results on sea-salt production, examines the performance of the modified function, and reports the implications of these results for the climate system.

5.1 Modifying the sea-salt generation function

Currently, the generation function of sea-salt aerosols takes into account two major dependencies influencing their formation—wind and size (equation (2.1) in §2.4.1). The wind dependence, $f(U_{10})$, is represented by the dependence of the whitecap coverage on wind speed, $W(U_{10})$, whose exact form is given with (2.3). Different analytical forms exist for the size dependence, $f(r_0)$, which usually models a

particle flux per unit area in a size bin, df/dr_0. Equation (2.1) is rewritten here to reflect this:

$$\frac{dF(r_0, U_{10})}{dr_0} = W(U_{10}) \cdot \frac{df}{dr_0} \qquad (5.1).$$

Modification of the current generation function (5.1) pertains to two aspects. The first aspect considers modifications aimed at inclusion of the effects of additional environmental variables, besides wind speed, on the sea-salt production, and generally changes the form of $W(U_{10})$. The second aspect considers modifications aimed at coverage of the entire size range of sea-salt aerosols relevant for climate studies, and changes the form of df/dr_0.

5.1.1 Include additional dependencies

The effect of additional variables on sea-salt production can be introduced in (5.1) by expanding $W(U_{10})$ to $W(U_{10}, \Delta T, T_s, S, f, d, C)$ (all variables defined in §2.5.1). This expansion can be achieved in two ways.

A first and straightforward way is to directly replace the estimates of W in (5.1) obtained using (2.3) with W values obtained by the new method. This approach can be considered empirical because it uses "measured" values for W retrieved from satellite-measured variables. The merit of this way of predicting sea-salt aerosol production is that the empirical W values intrinsically contain the effects of all possible environmental variables. Thus, the predicted sea-salt production can be expected to be more realistic than the production predicted by $W(U_{10})$ alone. When retrieved W values are not readily available, however, the necessity to gather different satellite-measured data in order to run the calculations of the new method (Chapter 3), could be an inconvenience.

A second way of including additional dependencies in the generation function is to replace $W(U_{10})$ in (5.1) with an analytical expression for $W(U_{10}, \Delta T, T_s, S, f, d, C)$ obtained using regression, or other, analysis from the whitecap coverage database (Chapter 4). In this case, W is estimated from routinely measured variables, e.g., U_{10}, T_s, and S. Yet, ΔT, f, d, and C remain inconvenient since their measurements are not routinely available (e.g., ΔT, f, and d) or are unavailable at all (e.g., C). The use of even only $W(U_{10}, T_s, S)$, however, could render more realistic estimates of sea-salt aerosol production than the use of $W(U_{10})$ alone.

However inconvenient the inclusion of additional variables in the generation function might be, it is a necessary scientific pursuit as the performance of the climate models continuously improves, yielding more stringent requirements for realistic and accurate predictions.

5.1.2 Extend toward smaller sizes

Sea-salt aerosol radii at formation, r_0, relevant for aerosol studies are in the range from 0.1 μm to 20 μm (§2.2.2, ***Size***). An evaluation of the current generation function (§2.4.3) showed that this function is applicable only in the upper end of the necessary size range of sea-salt aerosols, r_0 from 1.6 μm to 20 μm. An extension down to a particle radius of 0.1 μm is thus necessary.

The most rigorous way of extending the applicability of sea-salt generation function toward small sizes is to compile field measurements of sea-salt size distributions and extract an empirical expression. This approach proved successful when Monahan et al. (1986) and Andreas (1992) faced a similar problem with the necessity to extend the generation function toward larger droplets to include the production of spume droplets. Measurements of sea-salt aerosols with submicron sizes

are documented (Exton et al., 1985; O'Dowd et al., 1993; 1997; Reid et al., 2001) making this approach feasible. This option is not pursued here. Instead, as a first step in solving the small-size extension problem, this study uses readily available expressions for df/dr_0 .

The current generation function predicts the flux of sea-salt droplets over a wide range of r_0, from 1.6 μm to 500 μm, with four different analytical expressions in four size sub-ranges. Undoubtedly, the current generation function must be used to model df/dr_0 in the $1.6 \le r_0 \le 20$ μm range. All considerations in §2.4 justify this choice as the most appropriate one. Equation (2.2) clearly shows the exact analytical form of df/dr_0 in this range:

$$\frac{df}{dr_0} = 38\, r_0^{-0.024}\, \frac{df}{dr_{80}} \qquad (5.2a)$$

where term df/dr_{80} is (Andreas, 2002):

$$\log\left(\frac{df}{dr_{80}}\right) = 4.405 - 2.646\,(\log r_{80}) - 3.156\,(\log r_{80})^2 + 8.902\,(\log r_{80})^3 - 4.482\,(\log r_{80})^4$$

$$0.8 \le r_{80} \le 10 \ \text{μm} \qquad (5.2b).$$

The question at hand now is what functions to use to cover the sea-salt aerosol sizes in the r_0-range from 1.6 μm down to 0.1 μm.

A direct application of (5.2) for $r_{80} < 0.8$ μm (i.e., $r_0 < 1.6$ μm) does not work well: the argument log r_{80} in (5.2b) becomes negative for $r_{80} < 1$ μm rendering the flux of droplets too small (the solid line in Figure 5.1) while the expected behavior of df/dr_0 is an increase of the flux for small sizes.

A logical alternative is the well-known expression of Monahan et al. (1986), which is the best available one for the bubble-mediated production of sea-salt

droplets (Andreas, 1998). The size function of Monahan et al. (1986) is an appropriate choice because most sea-salt droplets at submicron radii are film and jet droplets produced exclusively by bubble bursting; spume droplets are larger and their presence at these sizes is not expected.

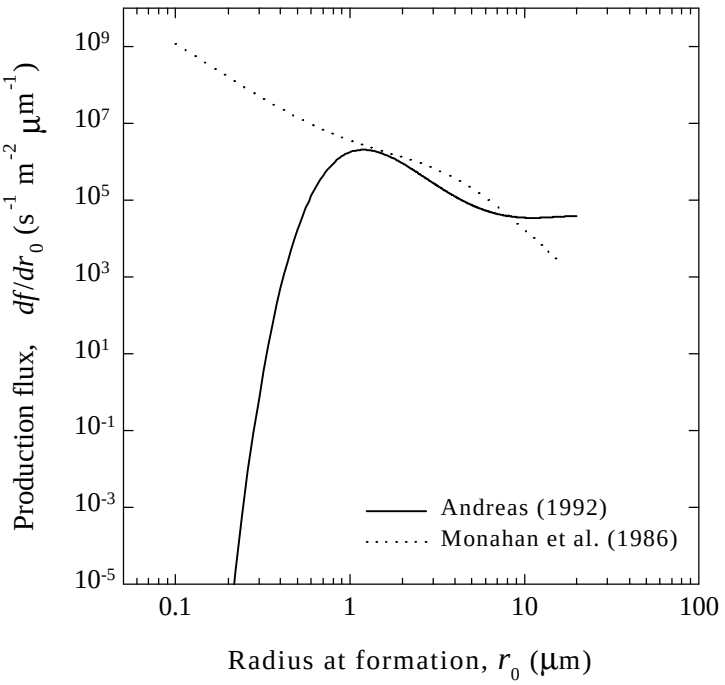

Figure 5.1 Size distributions, df/dr_0, modeled with Andreas (1992) and Monahan et al. (1986) functions over size range of 0.1 - 20 μm.

Monahan et al. (1986) give the bubble-mediated generation function in terms of r_{80}. The expression of Monahan et al. (1986, his equation 12) is represented in a form similar to (5.1) with two steps: i) the wind dependence, $W(U_{10})$, is clearly separated and excluded from the size dependence, df/dr_{80} ; ii) df/dr_{80} is converted to

df/dr_0 using relations derived by Andreas (1992, eqs. 15-17). As a result, the Monahan et al. (1986) size dependence, df/dr_0, can be written as:

$$\frac{df}{dr_0} = 0.506\, r_0^{-0.024}\, \frac{df}{dr_{80}} \tag{5.3a}$$

where the term df/dr_{80} is (Monahan et al., 1986):

$$\frac{df}{dr_{80}} = 35.74\times 10^4 r_{80}^{-3}\left(1+0.057\, r_{80}^{1.05}\right)10^n$$

$$n = 1.19\, e^{-B^2} \tag{5.3b}$$

$$B = \frac{0.38 - \log r_{80}}{0.65}$$

Caution is required when using (5.3b) since, similarly to (5.2b), its applicability domain is $0.8 \le r_{80} \le 8$ μm, i.e., $1.6 \le r_0 \le 16$ μm (Monahan et al., 1982). In contrast to (5.2b), however, (5.3b) behaves as expected for $r_{80} < 0.8$ μm: the flux of droplets increases at small sizes (the dotted line in Figure 5.1). Having found a function that behaves properly, the question now is: How far down in the small-size domain this function can be applied and still predict the droplets flux correctly. The results of Gong et al. (1997a) give a hint to the answer of this question.

In their model, Gong et al. (1997a) used the Monahan et al. (1986) function applying it for dry radii, r_d, as low as 0.03 μm (according to Andreas (2002), $r_d = 2\, r_{80} = 4\, r_0$). Gong et al. (1997a) observe a deviation of the Monahan et al. (1986) function from measurements beyond the applicable limit of $r_{80} = 0.8$ μm. Yet, the extension seems to work tolerably for sizes down to $r_d = 0.1$ μm (i.e., $r_{80} = 0.2$ μm and $r_0 = 0.4$ μm). The conclusion, therefore, is that the size dependence of Monahan et al.

(1986) could be extended with acceptable results in the range $0.2 \le r_{80} < 0.8$ μm (or $0.4 \le r_0 < 1.6$ μm).

The size dependence, df/dr_0, described with (5.2) and (5.3), can be used to cover droplet radii, r_0, from 0.4 to 20 μm. Still, the coverage of the smallest radii, 0.1 to 0.4 μm, remains an open question since there is not an expression readily available for these sizes. The rigorous approach using field measurements is the only appropriate way of solving the problem, and is left for now for future work.

Figure 5.2a plots the size distributions (5.2) (solid line) and (5.3) (dotted line) over their respective domains of applicability. There is a small difference

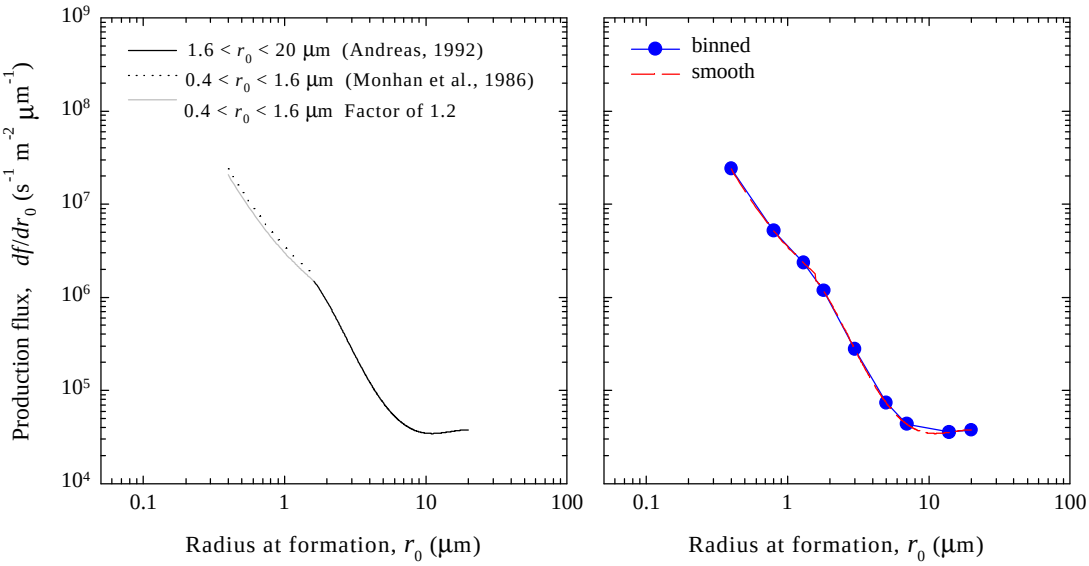

Figure 5.2 a) Connected size distributions over $0.4 < r_0 < 20$ μm range; b) Binned size distribution.

between the two functions at the connecting radius: at r_0 = 1.6 μm, the Monahan et al. (1986) function predicts higher value than the Andreas (2002) function does. Some

adjustment could be made to join the size distributions, df/dr_0, over the two sub-ranges smoothly. It is logical to seek adjustments to the Monahan et al. (1986) function, (5.3), for two reasons. First, the Andreas (2002) function, (5.2), is part of the current generation function, which is established as the most reliable one. Second, (5.3) is an extension of the Monahan et al. (1986) function in a range beyond its intended application, and deviations in its predictions are inevitably expected. Monahan et al.'s value of df/dr_0 at r_0 = 1.6 μm is a factor of 1.2 higher than that of Andreas' df/dr_0. The factor is not high, which is an assurance that the extension toward smaller sizes would yield acceptable results. Yet this factor is used to lower all df/dr_0 values obtained with (5.3) for r_0 < 1.6 μm. The result of this adjustment is shown in Figure 5.2a with a gray line.

5.1.3 Modified generation function

Putting together the modifications described above, the general form of the sea-salt generation function (5.1) transforms to:

$$\frac{dF}{dr_0} = W(U_{10}, \Delta T, T_s, S, f, d, C) \cdot \left(\frac{df}{dr_0} \right)_1 \qquad 1.6 \le r_0 \le 20 \ \mu\text{m} \quad (5.4a)$$

$$\frac{dF}{dr_0} = W(U_{10}, \Delta T, T_s, S, f, d, C) \cdot \left(\frac{df}{dr_0} \right)_2 \qquad 0.4 \le r_0 < 1.6 \ \mu\text{m} \quad (5.4b)$$

where (5.2) and (5.3) give $(df/dr_0)_1$ and $(df/dr_0)_2$, respectively.

5.2 Sea-salt aerosols from the modified generation function

This section reports results for computing sea-salt aerosol production and examines the performance of the modified sea-salt generation function. Sea-salt aerosol production is calculated with the modified generation function (5.4), using the

tabulated size distribution, df/dr_0 (Table 5.1), and the monthly W maps directly retrieved with the new method.

Though the use of monthly W maps calculated from the regression expression (4.11) is a fair alternative, it is not applied here because (4.11) needs further work and refinement.

Useful computational procedures are first described.

Table 5.1 Tabulated size distribution, df/dr_0, over binned $0.4 < r_0 < 20$ μm range.

Sub-range μm Equation	Bin No.	Bin width r_0 μm	Bin center r_0 μm	Bin width r_{80} μm	Bin center r_{80} μm	$(df/dr_0)_i$ i = 1, 2 s^{-1} m^{-2} μm^{-1}
0.4 - 1.6 (5.3)	1	0.2–0.6	0.4	0.1–0.3	0.2	2.397×10^{7}
0.4 - 1.6 (5.3)	2	0.6–1.0	0.8	0.3–0.5	0.4	5.167×10^{6}
0.4 - 1.6 (5.3)	3	1.0–1.6	1.3	0.5–0.8	0.65	2.337×10^{6}
1.6 - 20 (5.3)	4	1.6–2.0	1.8	0.8–1.0	0.9	1.177×10^{6}
1.6 - 20 (5.2)	5	2.0–4.0	3.0	1.0–2.0	1.5	2.767×10^{5}
1.6 - 20 (5.2)	6	4.0–6.0	5.0	2.0–3.0	2.5	7.358×10^{4}
1.6 - 20 (5.2)	7	6.0–8.0	7.0	3.0–4.0	3.5	4.335×10^{4}
1.6 - 20 (5.2)	8	8.0–20.0	14.0	4.0–10.0	7.0	3.554×10^{4}

5.2.1 Computational procedures

Binning of the size range

To facilitate numerous calculations over different drop radii, yet keep the shape of the size distribution intact, the range from 0.4 to 20 μm is divided in 8 bins. The bin widths and centers in r_0 and r_{80} terms are listed in Table 5.1. For each bin, respective df/dr_{80} and df/dr_0 are calculated with (5.3) or (5.2), obtaining terms $(df/dr_0)_1$ and $(df/dr_0)_2$ in (5.4), Table 5.1. Figure 5.2b shows that the binned size

distribution (blue) follows closely the size distribution (red) calculated with a smaller step, indicating that the choice of the bins is appropriate.

Monthly maps of *W* are prepared by summing up the daily *W* maps retrieved with the new method. The use of monthly instead of daily maps does not entail significant, if any, changes in the computation of sea-salt production maps because the terms $(df/dr_0)_1$ and $(df/dr_0)_2$ are constants within each bin and relations (5.4) are linear. This means that monthly aerosol loadings obtained by averaging daily sea-salt aerosol maps would not differ from monthly aerosol loadings computed using averaged monthly maps of *W*.

When the monthly *W* maps and the tabulated size distributions for each bin are prepared, they are plugged into (5.4) to obtain monthly size-segregated maps of sea-salt droplet production.

Sea-salt production in various terms

A host of quantities can be calculated from the sea-salt production maps convenient for comparison with others' measurements and calculations.

The initially calculated quantities are monthly *number fluxes* of sea-salt droplets within each size bin *i*, $(dF/dr_0)_i$ (i = 1,…, 8), in [s^{-1} m^{-2} μm^{-1}].

The flux at the radius of formation r_0, dF/dr_0, can be converted to fluxes proper for deliquescent or dry particles, dF/dr_{80} or dF/dr_d, respectively, with the Andreas (1992) relations. A representation of $dF/d(\log r_0)$ can be obtained from dF/dr_0 by multiplying dF/dr_0 with Δr_0 and dividing by $\Delta(\log r_0) = \log r_{max} - \log r_{min}$, where r_{max} and r_{min} are the upper and lower limits of each size bin (Table 5.1).

Summing up the number fluxes over all size bins gives a *total number flux* in [s^{-1} m^{-2}]:

$$dF = \sum_{i=1}^{8} \left(\frac{dF}{dr_0} \right)_i (\Delta r_0)_i \qquad (5.5a)$$

where $(\Delta r_0)_i$ is the width of each size bin.

Averaging the total fluxes $(dF)_k$ for all pixels on a map of sea-salt aerosol production produces *globally-averaged total fluxes*:

$$\overline{F} = \frac{1}{N} \sum_{k=1}^{N} (dF)_k \qquad (5.5b)$$

where N is the number of pixels representing the ocean surface.

The summation of the total fluxes $(dF)_k$ for all pixels over the sea-salt aerosol maps gives a *global number flux* in [s^{-1}]:

$$F = \Delta A \sum_{k=1}^{N} (dF)_k \qquad (5.5c)$$

where ΔA is the area of one pixel. Since the grid of the maps is 0.5°×0.5°, i.e., each pixel is a square with average side of 55.6 km, $\Delta A = 3.09 \times 10^9$ m^2.

Size-segregated number fluxes, dF/dr_0, can be converted into surface [m^2 s^{-1} m^{-2} μm^{-1}], volume [m^3 s^{-1} m^{-2} μm^{-1}], or mass [kg s^{-1} m^{-2} μm^{-1}] fluxes using weighting factors $4\pi r_0^2$, $(4\pi/3) r_0^3$, and $(4\pi/3) r_0^3 \rho$, where ρ is the density of sea-salt droplet; for fresh droplets at the moment of formation ρ = 1027 kg m^{-3}, while for deliquescent droplets at 80% RH ρ = 1197 kg m^{-3} (Moldanová and Ljungström, 2001, their Table 3). Total and global surface, volume, or mass fluxes are calculated analogously to (5.5).

The number concentration for each size bin i, $(dN/dr_0)_i$ (i = 1,…, 8) in [m^{-3} μm^{-1}], can be computed using the size-segregated number fluxes, $(dF/dr_0)_i$, and the deposition velocity, V_d (Smith et al., 1993):

$$\left(\frac{dN}{dr_0}\right)_i = \left(\frac{1}{V_d}\right)_i \left(\frac{dF}{dr_0}\right)_i \qquad (5.6).$$

The procedure of computing the deposition velocity is described in Appendix D. Again, total and global number concentrations in [m^{-3}], as well as surface [m^2 m^{-3}], volume [m^3 m^{-3}], or mass [kg m^{-3}] concentrations can be calculated similarly to their flux counterparts.

5.2.2 Results

Sea-salt aerosol loadings

Monthly maps (0.5°×0.5°) of sea-salt aerosol loadings for 1998 in terms of various variables are computed. For each month, HDF files for number flux, surface flux, volume flux, mass flux, number concentration, and mass concentration of sea-salt aerosols are produced. The monthly file for each of these variables contains 9 records, one for each size bin plus a record of total (over all sizes) flux or concentration. Monthly files with deposition velocity for each size bin are also stored. Monthly maps of number flux computed with the current generation function (Andreas, 2002), employing the wind-speed formula for *W*, are computed as well. These files comprise a rich database for sea-salt aerosol production. Table 5.2 lists the global averages of most computed variables for March 1998 in all size bins (surface flux is not included). Note that these values are for *fresh* sea-salt aerosols with radii at formation, r_0. The total amount of sea-salt aerosols produced by the world oceans is around 2×10^{16} g yr^{-1}. This value, though at the upper limit, is in the expected range (§2.2.2, ***Flux***).

Table 5.2 Global averages of sea-salt aerosol production by size in various terms for March 1998.

Size bin	Number flux $m^{-2}\ s^{-1}\ \mu m^{-1}$ From wind	Number flux $m^{-2}\ s^{-1}\ \mu m^{-1}$	Volume flux $m^3\ m^{-2} s^{-1} \mu m^{-1}$	Mass flux $kg\ m^{-2} s^{-1} \mu m^{-1}$	Number concentr. $m^{-3} \mu m^{-1}$	Mass concentr. $kg\ m^{-3} \mu m^{-1}$	V_d $m\ s^{-1}$
1	2.557×10^{5}	6.422×10^{5}	1.444×10^{-13}	1.479×10^{-10}	8.21×10^{9}	1.89×10^{-6}	4.12×10^{-5}
2	5.222×10^{4}	1.312×10^{5}	2.486×10^{-13}	2.545×10^{-10}	1.10×10^{9}	2.13×10^{-6}	7.08×10^{-5}
3	2.308×10^{4}	5.796×10^{4}	4.889×10^{-13}	5.005×10^{-10}	2.42×10^{8}	2.09×10^{-6}	1.49×10^{-4}
4	1.460×10^{4}	3.667×10^{4}	8.412×10^{-13}	8.612×10^{-10}	8.63×10^{7}	2.03×10^{-6}	2.68×10^{-4}
5	3.356×10^{3}	8.428×10^{3}	9.301×10^{-13}	9.523×10^{-10}	6.55×10^{6}	7.40×10^{-7}	8.53×10^{-4}
6	8.620×10^{2}	2.166×10^{3}	1.150×10^{-12}	1.177×10^{-9}	4.48×10^{5}	2.44×10^{-7}	3.22×10^{-3}
7	5.050×10^{2}	1.269×10^{3}	1.895×10^{-12}	1.940×10^{-9}	1.35×10^{5}	2.06×10^{-7}	5.79×10^{-3}
8	4.220×10^{2}	1.060×10^{3}	1.335×10^{-12}	1.367×10^{-8}	5.31×10^{4}	6.84×10^{-7}	1.33×10^{-2}

Figure 5.3 plots the size distribution of globally averaged number flux, dF/dr_0, at selected wind speeds for March 1998. Over the size range, the flux changes from 1×10^{3} to 1×10^{6} # $\mu m^{-1}\ m^{-2}\ s^{-1}$. An increase of the production flux with increasing wind speed is evident, especially for the lowest (5 m s^{-1}) and highest (20 m s^{-1}) winds. Yet the wind dependence exhibited in Figure 5.3 is weak; the curves for winds of 10 and 15 m s^{-1} practically coincide.

The suppression of the wind influence is certainly a result of the effect of sea surface temperature (SST) on whitecap formation and sea-salt aerosol production. Close scrutiny of U_{10} and T_s maps for March 1998 shows that all places over the globe with wind speed of U_{10} = 10 m s^{-1} are also places with SST values predominantly above 15 °C and peaking around 27 °C, while places with U_{10} = 15 m s^{-1} are in waters with

temperature below 12 °C with a peak around 5 °C. In other words, whitecaps under high winds but in cold water produce the *same* amount of sea-salt aerosols as whitecaps under lower winds but in warm water. This statement holds true for other months in spite of slight changes associated with seasonal variations of wind and SST values. Of course, a comparison of sea-salt fluxes at *different* wind speeds in locations with *similar* water temperature would reveal stronger wind dependence.

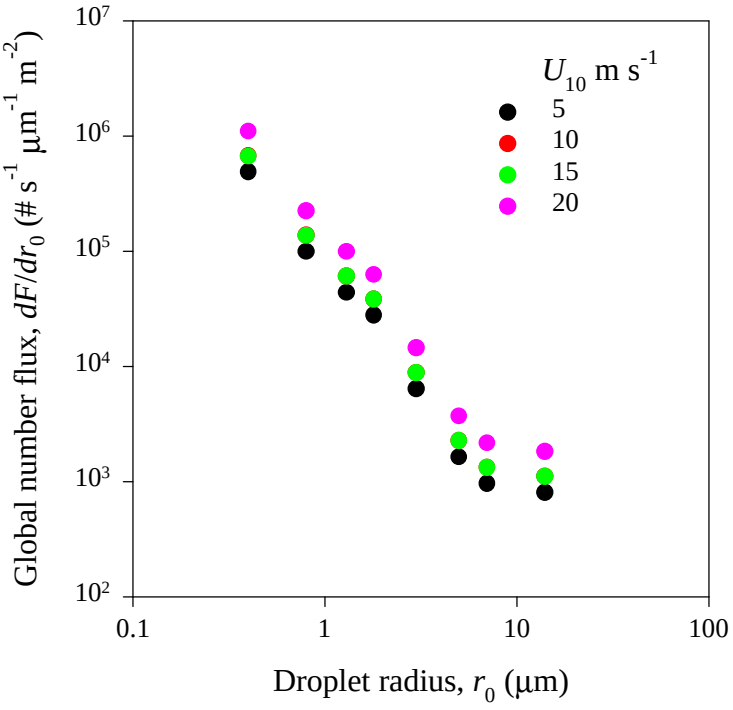

Figure 5.3 Size distribution of globally averaged number flux, dF/dr_0, for selected wind speeds.

The weak wind dependence in Figure 5.3 can also be explained with the size of the droplets. The droplets considered here have sizes below 20 μm. Usually, as

wind speed increases, prominent changes in sea-salt fluxes are observed for large particles since spume drops start to appear. Fluxes of smaller jet and film droplets may not show such prominent changes because they are bound with the whitecaps, whose appearance may not increase much with wind if the water is cold. Smith et al. (1993) report field measurements of sea-salt number concentrations, dN/dr_{80}, and derive number fluxes, dF/dr_{80}, from them. Their results indeed show stronger wind dependence for large particles and weaker wind dependence for small particles.

The number concentration, dN/dr_0, of freshly generated sea-salt droplets for March 1998, delivered to the atmosphere from sea-salt number flux, dF/dr_0, is shown in Figure 5.4a. Figure 5.4b shows the sea-salt mass, dm/dr_0 (kg m^{-3} μm^{-1}),

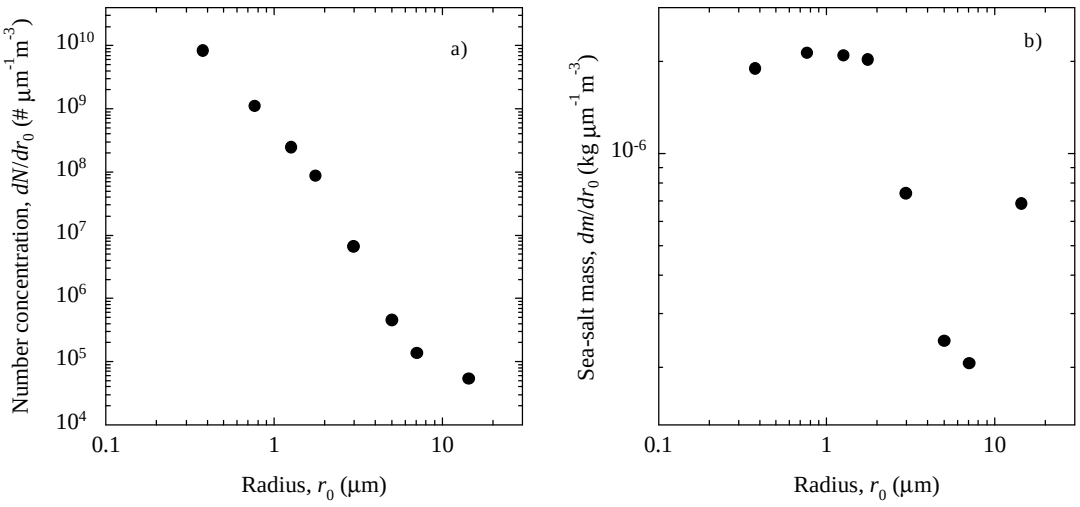

Figure 5.4 Size distributions of globally averaged number (a) and mass (b) concentrations of sea-salt aerosols.

corresponding to the concentration in Figure 5.4a. The trend of the mass concentration in Figure 5.4b differs from the typical one. Generally, though fewer in numbers, the

particles in the large-size end provide most of the sea-salt mass in the atmosphere (Smith et al., 1993; Gong et al., 1997a). Figure 5.4b shows an opposite trend. Though not typical, this trend is to be expected from the steep size distribution of the number concentration in panel a. In addition, the largest particles (above 20 μm), whose mass might bring the expected increase, are not considered here.

Spatial distribution of sea-salt aerosols

Figure 5.5 displays a global map of number flux of freshly generated sea-salt droplets for March 1998. Globally, the total (i.e., over all sizes) fluxes range from 1×10^5 to 1×10^6 # μm^{-1} m^{-2} s^{-1}. The highest fluxes are observed within the trade wind zones; the lowest are along the west coasts of the continents. Such spatial

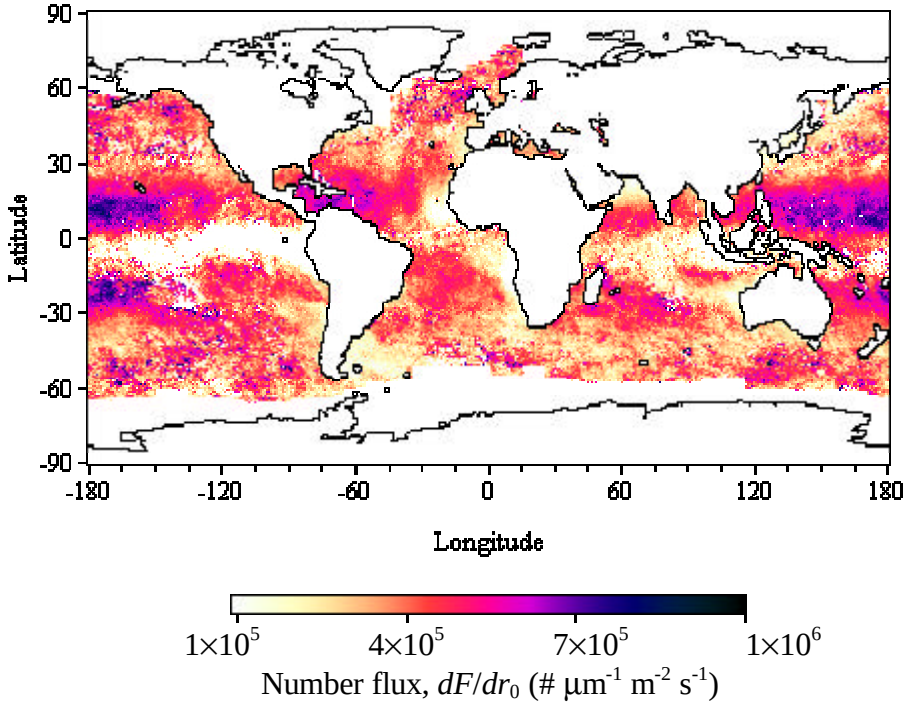

Figure 5.5 Total number flux, dF/dr_0, for March 1998 (map 0.5°×0.5°).

distribution, not surprisingly, is similar to that of the whitecap coverage plotted in Figure 4.2.

This spatial distribution of sea-salt aerosols corroborates beautifully the results of the Haywood et al. (1999) modeling discussed briefly in Chapter 2. Haywood and his colleagues map the difference between GCM computations and ERBE satellite observations of the annual-mean clear-sky solar irradiance reflected at

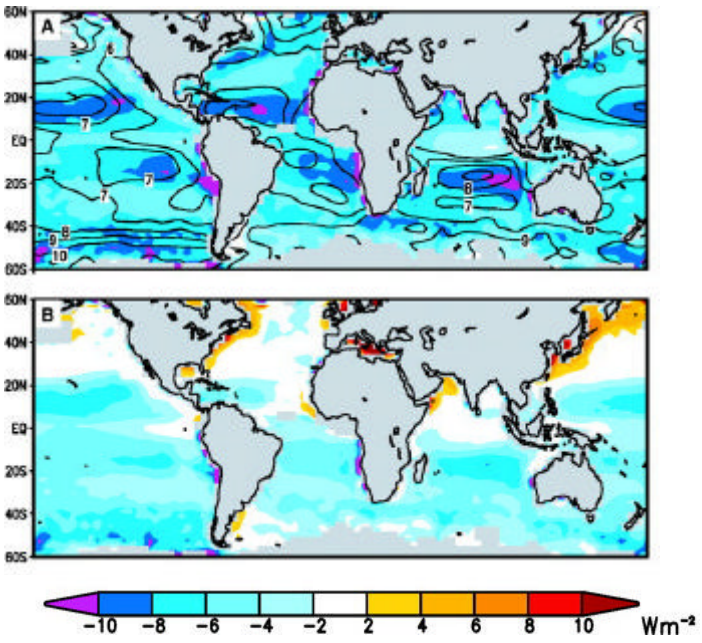

Figure 5.6 Difference in solar irradiance between model and observations: a) no aerosols considered; b) various aerosols, except sea-salt, considered. From Haywood et al. (1999).

the top of the atmosphere first without considering aerosols (Figure 5.6a) and then with all aerosol types included, except sea-salt aerosols (Figure 5.6b). The underestimation of the solar irradiance in Figure 5.6a shows peaks and valleys in the same places where

there are peaks and valleys in the sea-salt aerosol production (Figure 5.5). The fact that most of the underestimation remains when aerosols different from sea-salt are considered (Figure 5.6b) unambiguously proves that the major missing reflective component in Figure 5.6a is due to sea-salt aerosols.

The uniform spatial distribution of whitecap coverage over the globe revealed from satellite-derived *W* (noted and discussed in Chapter 4, Figure 4.2) reflects on the spatial distribution of sea-salt production as well. The latitudinal variations of sea-salt fluxes show this characteristic well (Figure 5.7). Panel a in the

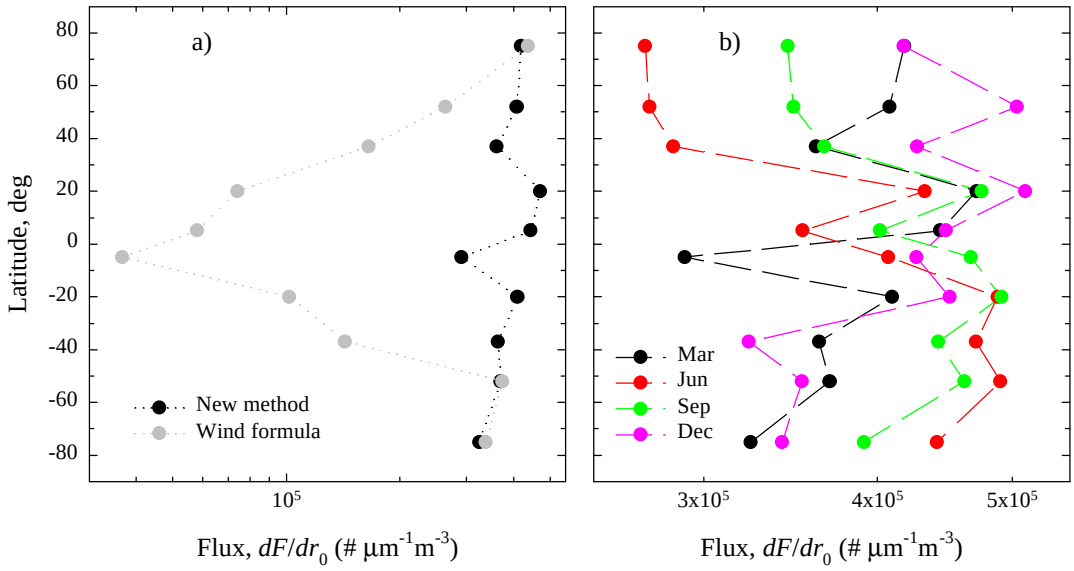

Figure 5.7 Latitudinal variations of sea-salt production flux: a) Comparison to the flux calculate using wind speed; b) Seasonal variations in the latitudinal patterns.

figure compares the number fluxes, $dF/dr_{0,}$ obtained with the new method and wind-speed formula for *W* in the current generation function. The fluxes plotted are

the average fluxes for several latitudinal zones. While the fluxes computed with *W* values from the wind-formula show a systematic decrease from high toward low latitudes (gray circles in panel a), fluxes computed with *W* from the new method shows similar values for high and mid latitudes (black circles in panel a). The lowest fluxes are along the equator.

Temporal distribution of sea-salt aerosols

Monthly and globally averaged values of total (i.e., over all sizes) sea-salt aerosol production for different terms are given in Table 5.3. The numbers are for fresh sea-salt aerosols with radii at formation r_0. Panel b in Figure 5.7 shows the

Table 5.3 Monthly averaged total sea-salt aerosol production in various terms.

Month	Number flux $m^{-2}\ s^{-1}$ from wind	Number flux $m^{-2}\ s^{-1}$	Volume flux $m^{-3}\ m^{-2}\ s^{-1}$	Mass flux $kg\ m^{-2}\ s^{-1}$	Number concentr. m^{-3}	Mass concentr. $kg\ m^{-3}$
January	1.490×10^{5}	4.081×10^{5}	1.744×10^{-10}	1.786×10^{-7}	4.032×10^{9}	1.479×10^{-5}
February	1.514×10^{5}	4.201×10^{5}	1.796×10^{-10}	1.838×10^{-7}	4.161×10^{9}	1.521×10^{-5}
March	1.574×10^{5}	3.952×10^{5}	1.689×10^{-10}	1.729×10^{-7}	3.918×10^{9}	1.426×10^{-5}
April	1.574×10^{5}	4.154×10^{5}	1.776×10^{-10}	1.818×10^{-7}	4.073×10^{9}	1.477×10^{-5}
May	1.448×10^{5}	4.096×10^{5}	1.750×10^{-10}	1.792×10^{-7}	4.041×10^{9}	1.474×10^{-5}
June	1.577×10^{5}	4.262×10^{5}	1.821×10^{-10}	1.865×10^{-7}	4.135×10^{9}	1.508×10^{-5}
July	1.699×10^{5}	4.379×10^{5}	1.872×10^{-10}	1.916×10^{-7}	4.221×10^{9}	1.531×10^{-5}
August	1.825×10^{5}	4.355×10^{5}	1.862×10^{-10}	1.906×10^{-7}	4.172×10^{9}	1.511×10^{-5}
September	1.770×10^{5}	4.433×10^{5}	1.895×10^{-10}	1.940×10^{-7}	4.253×10^{9}	1.550×10^{-5}
October	1.652×10^{5}	4.289×10^{5}	1.833×10^{-10}	1.877×10^{-7}	4.207×10^{9}	1.541×10^{-5}
November	1.535×10^{5}	4.221×10^{5}	1.804×10^{-10}	1.847×10^{-7}	4.176×10^{9}	1.535×10^{-5}
December	1.512×10^{5}	4.203×10^{5}	1.796×10^{-10}	1.839×10^{-7}	4.144×10^{9}	1.517×10^{-5}

fluxes obtained with the new method for four seasons. The lowest fluxes in the Northern hemisphere (boreal summer) are accompanied by the highest fluxes in the Southern hemisphere (austral winter), red line. In December (pink) the situation

reverses. March (black) and September (green) reflect the gradual change of the seasons.

Figure 5.8 depicts the 1998 seasonal variations of the total globally averaged mass flux, F_m, for both hemispheres. In the course of the seasonal cycles, F_m changes from a minimum of 155 μg m^{-3} μm^{-1} to a maximum of 214 μg m^{-3} μm^{-1}. The monthly fluxes in the SH are systematically higher than those in NH mostly due to the sea-salt production over the vast expanses of the Southern Ocean. As a result, the annual cycle on a global scale peaks during the austral winter and spring (July to October), and is minimum during the boreal winter and spring (January to May).

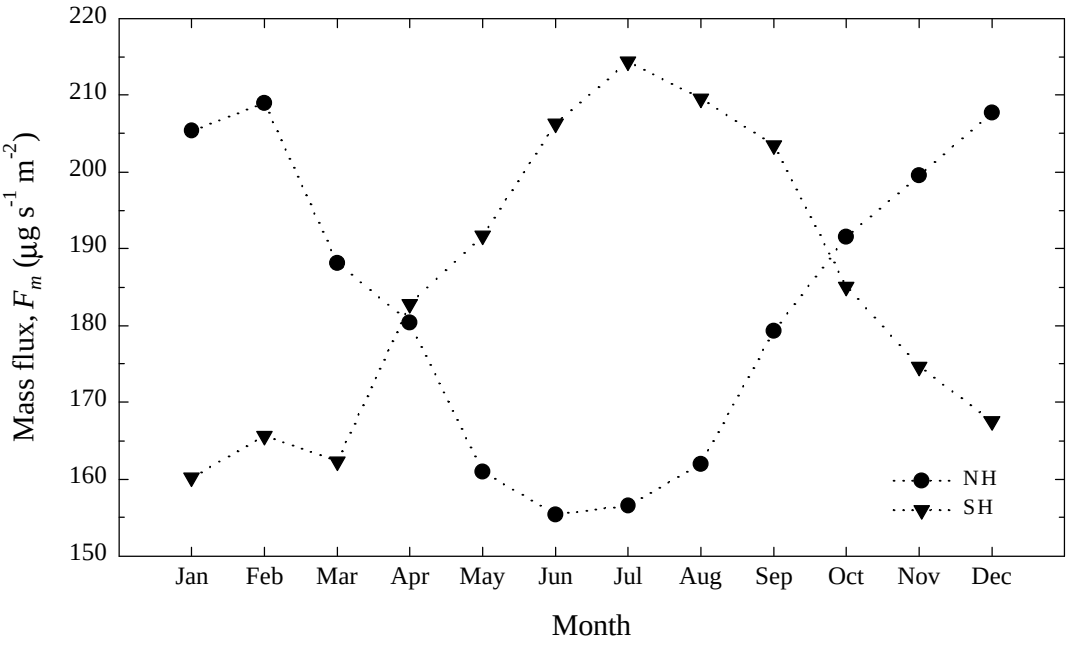

Figure 5.8 Seasonal variation of sea-salt mass flux for both hemispheres.

5.2.3 Performance of the modified generation function

The whitecap coverage values retrieved with the new method contain the effects of various environmental factors. The computed sea-salt aerosol flux is, therefore, expected to be more realistic than that predicted by other models, usually accounting for the effect of wind only. One way to check this expectation and judge the performance of the modified generation function is to compare the results of this study with observations of sea-salt aerosol production reported in the literature. If the results of this study are indeed more realistic, they would follow the observations closer than any other model.

Comparison with the current generation function

The comparison of the modified generation function with the current one is shown in Figure 5.9. The three curves in panel a of the figure are produced as follows. First, Andreas (2002) presents results with the current generation function (2.2) for sizes above $r_0 = 1.6$ μm in terms of volume flux; these are reproduced in Figure 5.9a (dotted line). In this case the wind dependence uses relation (2.3) with $U_{10} = 15$ m s^{-1}. Next, volume flux is calculated with (2.2) for sizes in the 0.4 – 20 μm range assimilating actual data (dashed line in Figure 5.9a). In this case the wind dependence uses relation (2.3) with the monthly averaged (March 1998) map of U_{10} (global average $U_{10} = 9.8$ m s^{-1}). The size dependence is provided by (5.2) for the 1.6 – 20 μm range and by (5.3) for the 0.4 – 1.6 μm range. As Figure 5.9a shows, volume fluxes from the current generation function for $U_{10} = 15$ m s^{-1} (dotted line) and actual data with average $U_{10} = 9.8$ m s^{-1} are consistent. These results, therefore, could serve as a reliable measure for the performance of the modified generation function. Finally, the monthly averaged map of W retrieved with the new method is plugged into the

modified generation function (5.4). The values obtained with the modified generation function (solid line in Figure 5.9a) are of the same order of magnitude as those from the current generation function, yet are higher by a factor of 2.5; in fact,

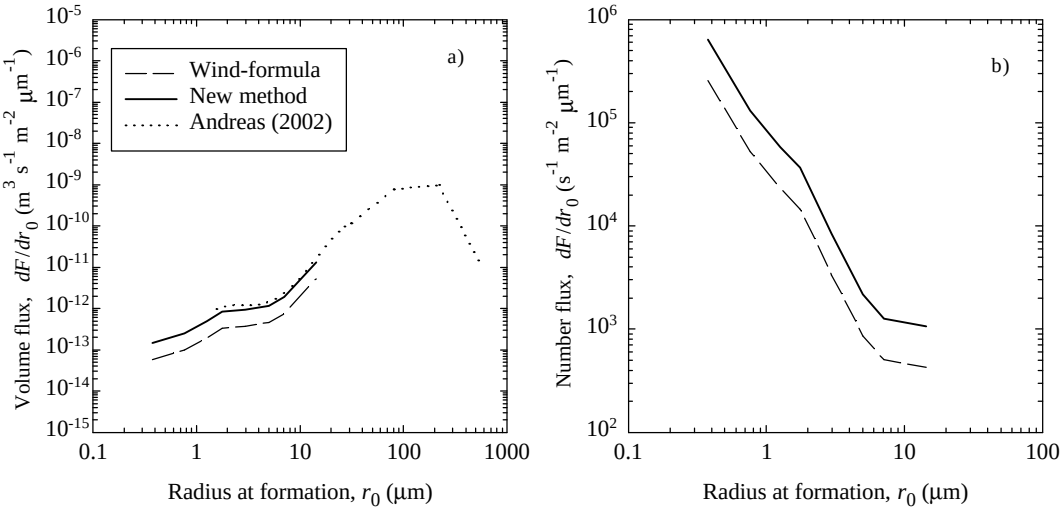

Figure 5.9 Comparison between current and modified generation functions: a) Volume fluxes calculated in three ways; b) Number fluxes.

they are closer to the 15 m s^{-1} curve of Andreas (2002). This difference of a 2.5-factor is expected, since *W* retrieved with the new method is 2.5 times higher than *W* obtained with the wind-speed formula (2.3). The probable reasons for this are discussed in Chapter 4 (end of §4.2.1). Number fluxes corresponding to these volume fluxes are presented in Figure 5.9b. Over the size range of 0.4 – 20 μm, the modified generation function yields number flux values from 1×10^3 to 6.4×10^5 (# m^{-2} s^{-1} μm^{-1}). Judging from the comparison with the current generation function and considering the reasons for the differences, it is concluded that the modified generation function credibly represents the flux of fresh sea-salt droplets.

Comparison with in situ observations

Comparing its results to observations can also demonstrate the performance of the modified generation function. Numerous measurements of the marine aerosol population are reported in the literature (Fitzgerald, 1991). However, a comparison with total marine aerosol flux or concentration, where "total" referrers to inclusion of many different aerosol species, may not yield plausible results because it is difficult to assess the contribution of the sea-salt component alone. Thus, measurements aiming at the sea-salt aerosol population specifically must be used. The following three comparisons are with experiments whose deliberate goal was measuring sea-salt aerosol production or concentration.

In March 1999, Reid et al. (2001) measured from aircraft the flux of whitecap-generated sea-salt particles at wind speeds of 4, 8, and 12 m s^{-1} in the vicinity of the North Carolina Outer Banks. Their data are plotted in Figure 5.10a (open symbols). Monthly averaged number fluxes for March 1998, averaged over an area encompassing their experimental flights were calculated with the modified generation function and also plotted in Figure 5.10a (solid circles). The average wind speed for the area of interested is 9.7 m s^{-1}. As the figure shows, the results of the modified function follow closely the Reid et al. (2001) values for wind speed of 12 m s^{-1}. The number flux at r_0 = 14 μm obtained with the modified function is higher than their value. This could be explained by the difficulties and high uncertainty experienced by Reid et al. (2001) in measuring the fluxes at large size. O'Dowd et al. (1997) also comment that there are experimental difficulties in measuring the sea-salt aerosol population, especially at the large-size end of the spectrum. Reid et al. (2001) compare their measurements at U_{10} = 8 and 12 m s^{-1} with the results of the Fairall et al. (1983), Monahan et al. (19860, and Smith et al. (1993) models. This study performs better

than the Fairall et al. (1983) and Smith et al. (1993) models and agrees with the Monahan et al. (1986) model (gray lines in Figure 5.10b), which compares most

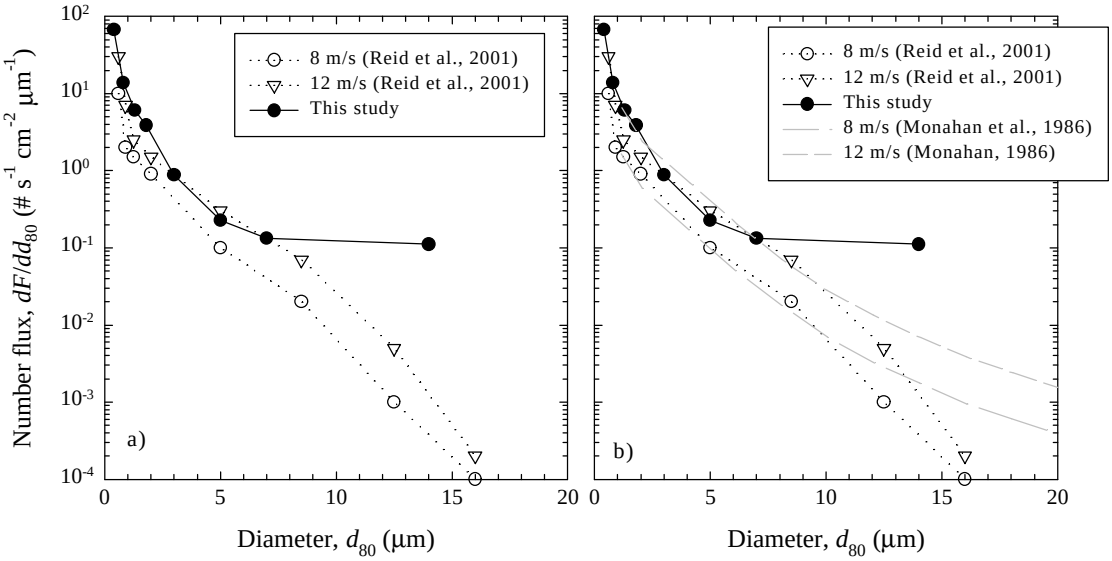

Figure 5.10 Comparison with sea-salt measurements reported by Reid et al. (2001):
a) Measurements and this study's calculations;
b) Monahan et al. (1986) model added.

favorably with Reid et al. (2001) measurements. It is reasonable for the Monahan et al. (1986) model to compute lower fluxes at large sizes than the modified generation function used in this study because it does not include the effect of spume drops at all, while the size dependence (5.2b) of the modified function does. The conclusion from the comparison with the Reid et al. (2001) data is that the modified generation function predicts sea-salt fluxes reliably and performs better than most other models.

The measurements of O'Dowd et al. (1997) in the North-East Atlantic in October and November 1989 provide comprehensive sea-salt size distributions. They were able to separate the sea-salt component from the other aerosol species employing a thermal analytical (volatility) technique. Their data of sea-salt concentration under U_{10} = 9 and 17 m s^{-1} and normalized to 80% RH are plotted in Figure 5.11. Assuming the climate is somewhat stationary, the modified generation function (5.4) was used to

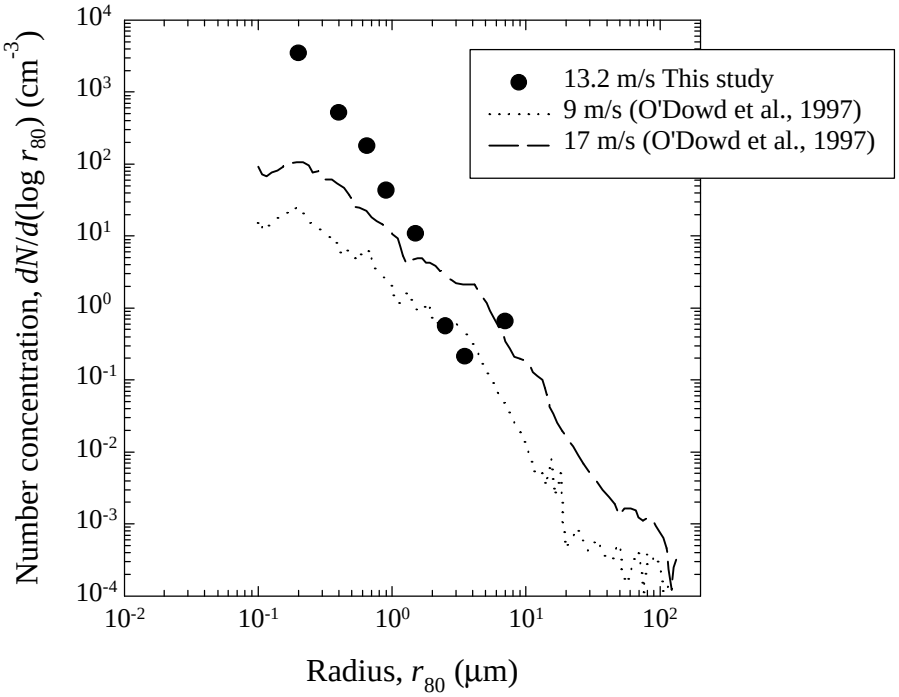

Figure 5.11 Comparison with sea-salt measurements reported by O'Dowd et al. (1997).

compute monthly averaged number concentration for 1998 and compare them with O'Dowd et al. observations from 1989. The concentrations estimated from the present study data are spatially averaged over the area of O'Dowd et al. measurements. The

mean wind speed for the months examined (October and November 1998) is 13.2 m s^{-1}. The resulting values of dN/dr_0 (μm^{-1} m^{-3}) are converted to $dN/d(\log r_{80})$ in units of cm^{-3} to match the O'Dowd et al. (1997) representation. These are compared to the O'Dowd et al. (1997) measurements in Figure 5.11 (solid circles). The comparison reveals that the concentrations obtained in this study are in order of magnitude agreement with the observations for the largest particles (r_{80} from 2 to 7 μm), and order of magnitude higher for smaller sea-salt aerosols. Since comparisons in Figures 5.9 and 5.10 show that the number fluxes generated with (5.4) are credible, a probable reason for the difference in Figure 5.11 could be the conversion obtained with (5.6). The deposition velocity (5.6) seems to be correctly calculated, as the discussions in Appendix D concludes. It is possible, however, that some important processes affecting the dry deposition of sea-salt particles are not taken into account in the model for estimating V_d, which leads to underestimation of V_d for small particles and overestimation of their concentration.

Smith et al. (1993) report size distributions of sea-salt concentrations for wind speeds from 0 to 30 m s^{-1}. Data were collected during several experiments at different times of the year and at different locations in the North Atlantic. Since the experimental site was near shore, the authors list the measures undertaken to assure that continental and anthropogenic aerosols, as well as aerosols produced by mechanism other than bubble-bursting within the whitecaps, are excluded from their dataset. The Smith et al. (1993) number concentrations for 5 and 30 m s^{-1} are shown in Figure 5.12 (open symbols). Number fluxes, annually averaged for 1998 and spatially averaged over the entire North Atlantic, were calculated with (5.4). The annual mean wind speed for the North Atlantic is 11.2 m s^{-1}.

The predictions of the modified generation function are much higher than the measurements, solid circles in Figure 5.12. There could be several reasons for the discrepancy. Once again, the conversion from number flux, dF/dr_0, to number concentration, dN/dr_0, with (5.6) could be a reason. In addition, Andreas (1998) already raised the issue that the Smith et al. (1993) observations were probably low by

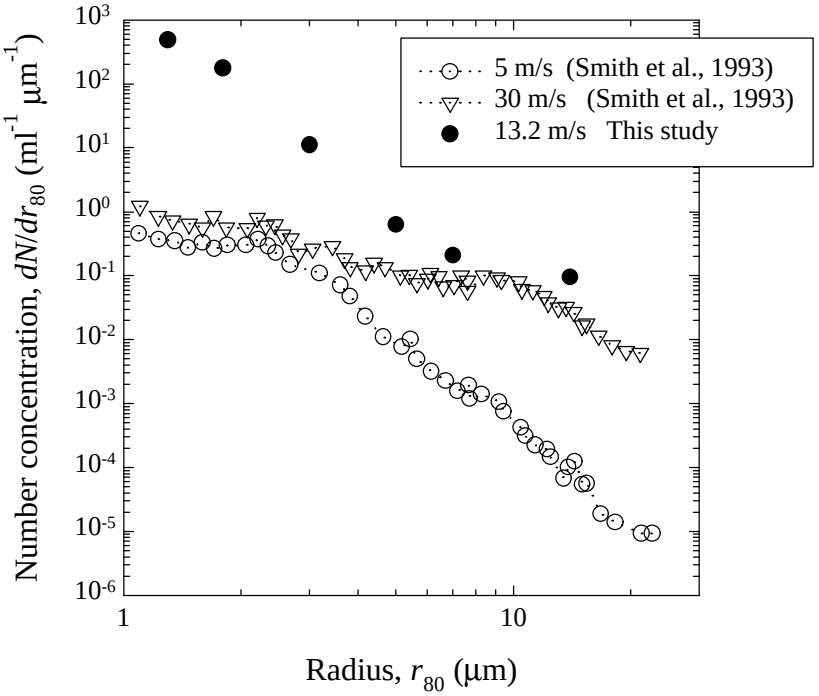

Figure 5.12 Comparison with sea-salt measurements reported by Smith et al. (1993)

at least a factor of 3.5. Finally, the solid circles in Figure 5.12 show the concentration of freshly generated sea-salt aerosols, while field observations, especially ones conducted over long periods of time, represent the steady state sea-salt concentration

in the atmosphere (Smith et al., 1993). The steady state concentration is a balance between many different processes affecting sea-salt aerosols (Gong et al., 1997a). These processes have not yet affected the concentrations predicted by this study and plotted in Figure 5.12.

Overall, one can conclude that the modified generation function estimates sea-salt production and concentration successfully.

5.3 Climate implications

Using the calculated sea-salt aerosol flux, it is possible to make rough estimations for the magnitude of the direct climate effect of sea-salt aerosols, the sea-salt contribution to the formation of CCN, and the concentration of different elements delivered into the atmosphere by chemical reactions on and within sea-salt aerosols.

Sea-salt loading in the atmosphere is a natural agent of the climate system since sea-salt aerosols are part of the natural tropospheric aerosols. Sea-salt aerosols control the properties of a clean marine atmosphere because they are the dominant species among the natural aerosols in remote oceanic areas. Therefore, the estimates described in the following sections have three useful aspects: i) they represent the contribution of sea salts to the natural state of the climate; ii) they set the baseline properties of the background atmosphere; iii) they yield an assessment of the climate forcing due to anthropogenic aerosols by the evaluation of changes around this baseline.

The models used to estimate the climate effects of sea-salt aerosols follow the models estimating the radiative forcing of anthropogenic aerosols. The radiative forcing is evaluated as the externally imposed perturbation in the radiative energy

budget of the Earth's climate system (IPCC, 2001). Anthropogenic aerosols usually perturb the Earth's energy budget by inducing change in the planetary albedo as their concentration increases. In contrast to the anthropogenic aerosols, sea-salt aerosols do not cause perturbation in the radiative energy budget. Being a natural component of the earth-atmosphere system, sea-salt aerosols have always been present in the atmosphere in some steady state concentration and have their own contribution to the radiative energy budget. This contribution represents the sea-salt aerosol effect, direct or indirect, on the climate system. Thus, rather than *perturbation*, the models below estimate the *contribution* of sea-salt aerosols to the planetary energy budget.

It is necessary to note that all estimates here are tentative. The aerosol effects on climate processes are currently under active investigation. New findings, measurements, models, and theory are constantly being reported. Thus, many of the values used for the estimations vary widely and often the choice of these values may change the estimates significantly. An attempt was made, unavoidably subjective, to choose values from the most widely cited and recognized sources.

5.3.1 Direct climate effect

Charlson et al. (1992) proposed a model estimating the magnitude of the direct effect of anthropogenic sulphate aerosols. Following the same concept, the model presented here estimates the albedo and the reflected mean shortwave radiation due to the globally and annually averaged steady-state concentration of sea-salt aerosols.

The mean shortwave radiation, $\overline{F_{RA}}$, reflected back to space by the natural loading of sea-salt aerosols could be expressed as:

$$\overline{F_{RA}} = -\frac{1}{4} F_T (1 - A_{cc}) \overline{A_{ss}} \tag{5.7}$$

where F_T = 1370 W m^{-2} is the solar constant, with F_T /4 giving the average amount of solar energy reaching Earth's surface, A_{cc} = 0.61 is the fractional cloud cover, and $\overline{A_{ss}}$ is the sea-salt aerosol contribution to the planetary mean albedo. The factor $(1 - A_{cc})$ is introduced because the sea-salt aerosol albedo is for clear sky areas over the ocean. The negative sign denotes that the direct effect of sea-salt aerosols cools the climate system. The sea-salt albedo can be represented as:

$$\overline{A_{ss}} \cong 2T^2 (1 - \overline{A_{os}})^2 \overline{b}\ \overline{t_{ss}} \tag{5.8}$$

where T = 0.76 is the atmospheric transmittance, $\overline{A_{os}}$ = 0.05 is the mean albedo of the underlying ocean surface (Pinet, 1992, Table 14-1), $\overline{b}$ = 0.29 is the fraction of the radiation scattered upward by the sea-salt aerosols, and $\overline{t_{ss}}$ is the sea-salt aerosol optical thickness defined as:

$$\overline{t_{ss}} = a_{ss} \overline{B_{ss}} \tag{5.9}$$

where a_{ss} = 2.5 m^2 g^{-1} is mass scattering efficiency and $\overline{B_{ss}}$ is the column burden of sea-salt aerosols (Haywood et al., 1999). The column burden, $\overline{B_{ss}}$ (g m^{-2}), is related to the annual mass flux, F_m = 2×10^{16} g yr^{-1}, and the residence time, t = 1 day, of the sea-salt aerosols in the atmosphere:

$$\overline{B_{ss}} = \frac{F_m t}{A} \tag{5.10}.$$

Here A = 3.65×10^{14} m^2 is the ocean area over which sea-salt aerosols are confined; A is estimated from the annual map of F_m.

Using (5.10) to (5.8), and the values cited for the various parameters, the column burden of the sea-salt aerosols is estimated to be $\overline{B_{ss}}$ = 150 mg m^{-2}, the sea-salt optical thickness is $\overline{t_{ss}}$ = 0.375, and the contribution of the sea-salt aerosols to the

planetary albedo is $\overline{A_{ss}}$ = 0.113. With (5.7), the shortwave radiation reflected by the sea-salt aerosols is $\overline{F_{RA}}$ = -15.53 W m^{-2}. This $\overline{F_{RA}}$ value is about a factor of 2 higher than the expected 8-10 W m^{-2} value in the Haywood et al. (1999) model necessary to balance the difference between computations and observations (Figure 5.6).

There are numerous possible reasons for the discrepancy between the estimates for the variables above and the estimates cited in the literature. One reason is the higher value of estimated whitecap coverage, *W*, obtained with the new method: a global average of about 3% instead of 1%, which yields higher estimates of F_m. Any improvement in estimating *W* would lead to refining the $\overline{F_{RA}}$ value. The values of mass-scattering efficiency, a_{ss}, may range from 0.68 to 8.7 m^2 g^{-1} (Quinn and Coffman, 1999) for different sea-salt aerosol sizes and at different latitudes. The column burden, $\overline{B_{ss}}$, could be obtained not only from (5.10) but also from sea-salt mass concentration and the height of the marine boundary layer (Quinn and Coffman, 1999) with the latter being measured or chosen differently by different investigators. This brings quite a wide range of values for $\overline{B_{ss}}$ (Tegen et al., 1997; Quinn and Coffman, 1999).

The optical thickness of sea-salt aerosols, $\overline{t_{ss}}$, could be considered as the optical thickness of a clean background atmosphere. If measurements of $\overline{t_{ss}}$ show variations around the sea-salt $\overline{t_{ss}}$-value, these variations can be attributed to changes in the aerosol loadings and would represent the direct climate forcing of the aerosols causing these changes.

5.3.2 Indirect climate effect

The indirect effect of sea-salt aerosols is manifested in: i) the amount of CCN formed on sea-salt aerosols; and ii) the contribution of the cloud droplets grown

from CCN formed on sea-salt particles to the cloud albedo. Estimates of these quantities folow.

CCN formed on sea-salt aerosols

Pruppacher and Klett (1978) propose an expression estimating the number of CCN, N_{CCN}, formed on particles with concentration N:

$$N_{CCN} = Ns^k \tag{5.11}$$

where s is the supersaturation, which for marine stratocumulus clouds has typical values of 0.2 - 0.3 % (O'Dowd et al., 1997), and $k \approx 0.7$ is an experimentally derived constant (Pruppacher and Klett, 1978).

The number concentration, N, of sea-salt aerosols is estimated in this study. The steady-state concentration of the sea-salt aerosols is evaluated as a 2% of N. At $N = 3.92 \times 10^9$ particles per m^3 for March 1998 (Table 5.3), the steady-state concentration of sea-salt aerosols is 157 particles per cm^3, which produces $N_{CCN} = 1.2$ CCN per cm^3. This value is in agreement with the estimates given by Andreae (1995) of around 1 particle per cm^3.

The use of the steady-state concentration of sea-salt aerosols to estimate the number of CCN formed on them, however, tends to underestimate their role in more dynamic settings with constantly blowing and changing winds. If the "instantaneous" concentration (i.e., N at r_0 without 2% fractioning) is used for the calculation with (5.11), the result is $N_{CCN} = 59$ CCN per cm^3. This value falls within the range of active CCN estimated by O'Dowd et al. (1997): from 5 particles per cm^3 at 5 m/s to 50 cm^{-3} at 15 m s^{-1} to 150 cm^{-3} at 20 m s^{-1}.

Effect on planetary albedo

This section describes the evaluation of the sea-salt aerosol contribution to the planetary albedo via the albedo of marine stratiform clouds containing cloud droplets, which have grown on sea-salt formed CCN. The calculation procedure follows the concept of the Charlson et al. (1992) model. Analogously to (5.7), the mean shortwave radiation reflected back to space by marine stratiform clouds, $\overline{F_{RC}}$, with mean albedo $\overline{A_c}$ is:

$$\overline{F_{RC}} = -\frac{1}{4} F_T A_{mst}\, 0.8\, \overline{A_c} \qquad (5.12),$$

where, F_T = 1370 W/m^2 is the solar constant, and A_{mst} = 0.448 is the fraction of the ocean area covered with stratiform clouds (Charlson et al., 1987). The factor of 0.8 in (5.12) comes from the consideration that ozone above the clouds absorbs the shortwave radiation, which lowers the total planetary albedo in comparison with the real albedo of the cloud $\overline{A_c}$ (Charlson et al., 1987).

The mean cloud albedo of a nonabsorbing, horizontally homogenous cloud is analytically approximated as:

$$\overline{A_c} = \frac{b(m_0)\, t_c / m_0}{1 + b(m_0)\, t_c / m_0} \qquad (5.13).$$

Here m_0 is the cosine of the solar zenith angle, $b(m_0)$ is the fraction of sunlight incident to the cloud at angle $q_0 = \cos^{-1} m_0$ that is scattered in the upward direction for a single-particle scattering, and t_c is the optical thickness of the cloud.

The cloud optical thickness is parameterized as $t_c = p\, r_e^2 Q_{ext} z_c N_{cd}$, where r_e is the effective cloud drop radius, Q_{ext} is the average extinction efficiency, z_c is the thickness of the cloud, and N_{cd} is the number concentration of cloud droplets. Since not enough information is available to estimate the drop sizes in marine stratiform

clouds, $_e$ could be expressed through the liquid water content, L , of these clouds, that is $L_c = (4/3)p\, r_e^3\, r\, N_{cd}$. This leads to

$$t_c = p\, Q_{ext} z_c \left(\frac{3L_c}{4pr} \right)^{2/3} N_{cd}^{1/3} \tag{5.14}$$

with $r \approx 1000$ kg m^{-3} being the density of pure water. Here Q_{ext} can be approximated with a constant ($Q_{ext} \approx 2$) assuming that the radii of the cloud droplets are much greater than the wavelength of visible light. The cloud droplets considered here easily meet this assumption since they grow on CCN formed on relatively large sea-salt aerosols. Marine stratiform clouds have typical thickness of $z_c \approx 500$ m and liquid-water content $L_c = 0.22$ g m^{-3} (Stephens, 1978a).

Currently, there is not a well-established relation between the number of CCN present in the atmosphere and the number of cloud droplets activated on them. Thus, the result from the previous section for the number of CCN formed on sea-salt aerosols cannot be used to obtain N_{cd}. On the basis of simultaneous measurements of aerosol and cloud droplet concentrations, O'Dowd et al. (1999) propose a parameterization of the number of cloud drops, N_{cd}, formed from sea-salt aerosols with concentration N, in cm^{-3}, for updraft velocity of 0.175 m s^{-1}:

$$\begin{aligned} N_{cd} &= A_1 (1 - e^{A_2 N}) \\ A_1 &= 365.16 - 2.038 U_{10} - 0.438 U_{10}^2 \\ A_2 &= -\left(2.481 - 0.049 U_{10} + 0.0053 U_{10}^2\right)/1000 \end{aligned} \tag{5.15}$$

The steady-state sea-salt concentration of $N = 78.4$ cm^{-3} for March 1998 produces $N_{cd} = 52$ cm^{-3} at wind speed $U_{10} = 12$ m s^{-1}. On the one hand, the order of magnitude of this N_{cd} value is valid because the number of cloud droplets in marine stratiform clouds formed on *any* CCN (not only on CCN formed from sea-salt aerosols) is in the

range from 120 to 440 cm^{-3} (Stephens, 1978a). On the other hand, it is generally known that only a part of the CCN present in the atmosphere grow to cloud droplets. This means that a value of 52 cm^{-3} for N_{cd} is not consistent with the values for CCN formed on sea-salt aerosols obtained in the previous section (1.2 CCN cm^{-3}). This is one of many examples demonstrating how far from settled is the work in the field of aerosol effects on clouds.

Plugging N_{cd} = 52 cm^{-3} and all remaining values in (5.14) gives an optical thickness t_c = 16.42 for marine stratiform clouds. Using the global-average zenith angle $q_0 = 60°$ (Charlson et al., 1987), $m_0 = \cos q_0 = 0.5$, and $b(m_0) = b(0.5) = 0.068$ at the estimated t_c value (Stephens, 1978b). With (5.13), the mean albedo of marine clouds is $\overline{A_c}$ = 0.69, yielding a reflection of, and hence a cooling by, $\overline{F_{RC}}$ = -84.7 W m^{-2}. The solar radiation reflected from the Earth's surface is on average around 102 W m^{-2} (Wielicki et al., 1995). This means that marine stratiform clouds are responsible for 83% of the reflected shortwave radiation over the oceans. Since the high albedo of these clouds is largely due to cloud drops grown on CCN formed on sea-salt aerosols, the indirect effect of sea salts on the climate is considerable.

5.3.3 Halogen chemistry

Sea-salt aerosols are major source of naturally emitted inorganic reactive halogens in both particulate and gaseous forms.

The mass of chlorine, Cl, and bromine, Br, entering the atmosphere via sea-salt drops can be estimated using the global annual flux of sea-salt mass concentration computed in this study, 2×10^{16} g yr^{-1}. The typical content of Cl and Br in seawater is 19.353 and 0.0673 g/kg, respectively (Pilson, 1998). These values are used

for the estimate of Cl and Br fluxes since fresh sea-salt aerosols have a chemical composition similar to that of the seawater (§2.2.1, ***Chemical composition***). Sea-salt aerosols deliver 1.1×10^{16} g yr^{-1} particulate Cl and 4×10^{13} g yr^{-1} particulate Br to the atmosphere.

Rapid acid-displacement reactions occur within the fresh alkaline (pH > 8) sea-salt aerosols. Sea-salt aerosols are dechlorinated in a matter of tens of seconds to about 15 minutes (Chameides and Stelson, 1992; Keene et al., 1998). At pH ≈ 6, Cl volatilizes from the aerosol to the gas phase, mostly in the form of HCl and $ClNO_2$ (Erickson et al., 1999). The Cl deficit in sea-salt aerosols ranges from 15 to > 80% depending on the location (coastal zone or open ocean) and the size of the sea-salt aerosols. This implies that the mass of gaseous Cl delivered into the atmosphere from the sea-salt aerosols is in the range of $(1.65 \text{ to } 8.8) \times10^{15}$ g yr^{-1}.

After the dechlorination, acid displacement reactions continue within the sea-salt aerosols until their pH drops below 4. Under these conditions, Br escapes from the aerosols and delivers gaseous Br to the atmosphere, mostly in the form of HBr. Chemical models predict 50 to 60% destruction of surface O_3 as a result of reactions involving gaseous Br. The information on these reactions as well as their modeling and observation are still scarce in the literature.

Chameides and Stelson (1992) propose a comprehensive chemical model investigating the coupling of the sulfur cycle with that of the sea-salt cycle. While the pH of the fresh sea-salt aerosols is high, sea-salt and non-sea-salt (nss) S within the aerosols is rapidly oxidized by O_3 leading to an accumulation of nss-SO_4^{2-}. Thus, the annual flux of sea-salt aerosols to the atmosphere creates a comparable flux of nss-SO_4^{2-}, that is, in order of 2×10^{16} g yr^{-1}. Being relatively large, sea-salt aerosols

return to the ocean and remove 10 to 100% of nss-SO_4^{2-} from the atmosphere, that is, sea-salt aerosols are sink for 10^{15} to 10^{16} g of nss-SO_4^{2-} annually.